Hindawi
Adsorption Science & Technology
Volume 2023, Article ID 9021169, 12 pages
https://doi.org/10.1155/2023/9021169

Research Article

NO_2 Gas Sensing Properties of Ag-Functionalized Porous ZnO Sheets

Min Young Kim,[1] Jeong Yun Hwang,[1] Ali Mirzaei,[2] Sun-Woo Choi,[3] Sang-il Kim,[4] Hyun-Sik Kim,[4] Sun-Jae Kim,[5] Jong Wook Roh,[6] Myung Sik Choi,[6] Kyu Hyoung Lee,[1] Seung Yong Lee,[1,7] and Changhyun Jin[1,7]

[1]*Department of Materials Science and Engineering, Yonsei University, Seoul 03722, Republic of Korea*
[2]*Department of Materials Science and Engineering, Shiraz University of Technology, Shiraz 71557-13876, Iran*
[3]*Department of Materials Science and Engineering, Kangwon National University, Samcheok 25913, Republic of Korea*
[4]*Department of Materials Science and Engineering, University of Seoul, Seoul 02504, Republic of Korea*
[5]*Faculty of Nanotechnology and Advanced Materials Engineering, Sejong University, Seoul 05006, Republic of Korea*
[6]*School of Nano & Materials Science and Engineering, Kyungpook National University, Sangju 37224, Republic of Korea*
[7]*KIURI Institute, Yonsei University, Seoul 03722, Republic of Korea*

Correspondence should be addressed to Seung Yong Lee; lsy549@yonsei.ac.kr and Changhyun Jin; z8015026@yonsei.ac.kr

Received 5 November 2022; Revised 23 December 2022; Accepted 31 December 2022; Published 19 January 2023

Academic Editor: Sami-ullah Rather

Herein, we report a simple and scalable synthesis route to prepare Ag-functionalized porous ZnO sheets and their enhanced NO_2 gas sensing properties. Porous ZnO sheets functionalized with well-dispersed submicron Ag particles were prepared by using a hydrothermal method-based one-pot synthesis route from Zn and Ag precursors. NO_2 gas sensing performance (response, selectivity, response time, and recovery time) was optimized at 200°C in the gas sensor fabricated with 3 at% Ag-functionalized porous ZnO sheets. We demonstrated a response (R_g/R_a) of 17.18 to 10 ppm NO_2 gas and also obtained a high response of 14.05 even at 60% relative humidity due to the synergetic effect of improved NO_2 gas adsorption in the presence of Ag particles and increased resistance by the formation of Schottky barrier at Ag-ZnO heterojunctions.

1. Introduction

Nitrogen dioxide (NO_2) is a red-brown highly oxidizing gas [1] and one of the major air pollutants [2], causes nose and respiratory problems, coughs, fatigue, eye irritation, and nausea, and affects patients with debilitating pulmonary system diseases [3–5]. It also makes severe environmental issues such as smog and acid rain [6, 7]; thus, the development of NO_2 gas sensors with high reliability and performance is urgently required.

ZnO is widely used gas sensing materials due to its semiconducting nature (E_g = 3.37 eV) with high electron mobility (200 $cm^2 V^{-1} s^{-1}$), nontoxicity, and high thermal stability [8, 9]. After the first report on the gas sensing properties of ZnO [10], many researches for gas sensing based on ZnO have been carried out [11, 12]. One of the main approaches to enhance the gas sensing properties of ZnO is morphological or dimensional control since gas adsorption is directly related to the surface area of gas sensing materials. Various forms of ZnO such as nanowires [13], nanorods [14], nanotubes [15], nanofibers [16], nanopetals [17], hierarchical architectures [18], nanosheets [19], and nanowalls [20] have been studied to improve gas sensing properties. However, a major obstacle in the application of ZnO-based gas sensor is poor selectivity of ZnO owing to the relatively good response to different gases [21]. To address this, decoration or functionalization of noble metal particles on ZnO surface, which improves the adsorption of gas molecules and forms a Schottky potential barrier [22, 23], is commonly used [24]. Among noble metal elements, Ag can be a good choice due to its low price, high electrical

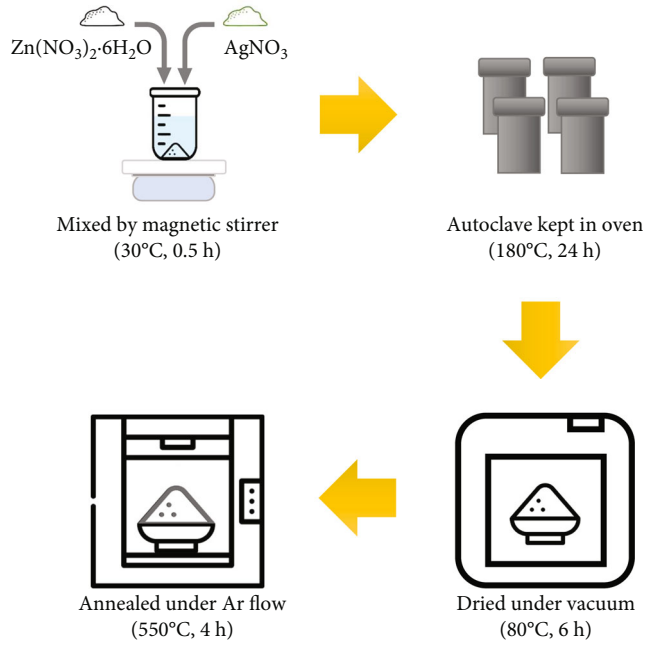

Figure 1: Schematic of the synthesis method.

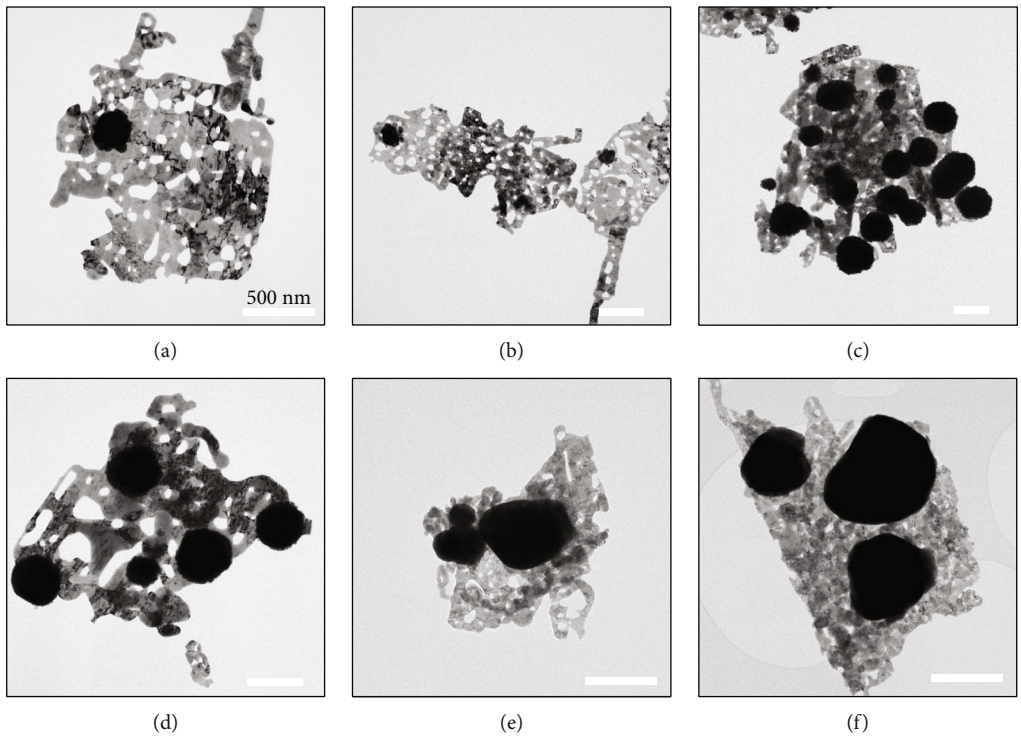

Figure 2: TEM images of the (a, b) 1, (c, d) 3, and (e, f) 5 at% Ag-functionalized porous ZnO sheets.

conductivity, and good catalytic performance [25, 26]. Yin et al. [27] and Wei et al. [22] reported the important roles of Ag particles on the sensing properties of one-dimensional ZnO structures to NO_2 and ethanol gases. In particular, there have been many studies on NO_2 gas sensing [28–32], but there are few reports on ZnO, which can simultaneously achieve a two-dimensional nanosheet cross-sectional area and a nanocomposite with Ag in a single process.

In the present study, we aimed to prepare hybrid materials of Ag particles and ZnO powders in an effort to improve the NO_2 gas sensing properties. Notably, by using hydrothermal method-based one-pot synthesis technique, well-dispersed submicron Ag particles (1, 3, and 5 at%) functionalized porous ZnO sheets were obtained from Zn and Ag precursors. NO_2 gas sensing properties including response, selectivity, response time, and recovery time were

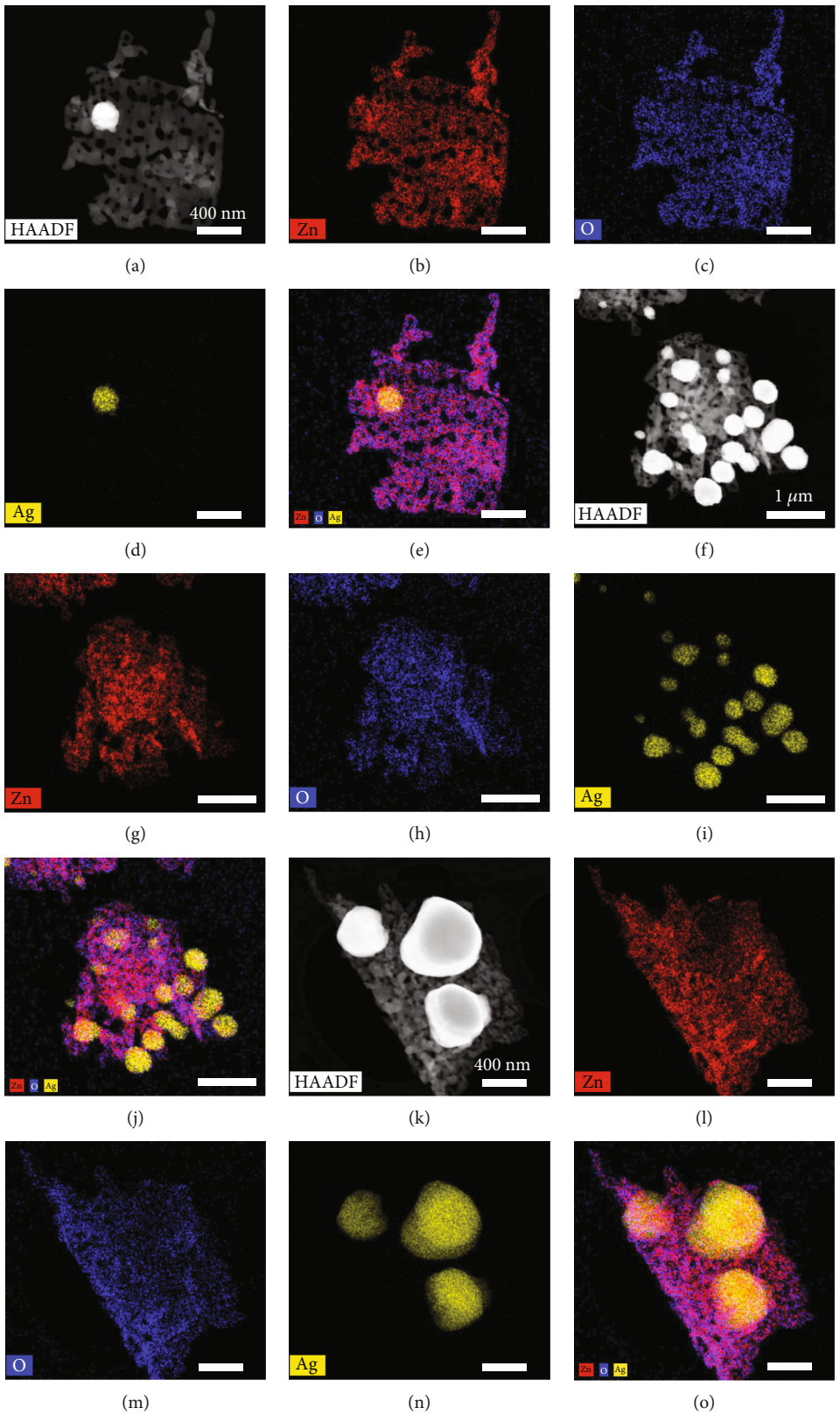

Figure 3: TEM elemental mapping of the (a–e) 1, (f–j) 3, and (k-o) 5 at% Ag-functionalized porous ZnO sheets.

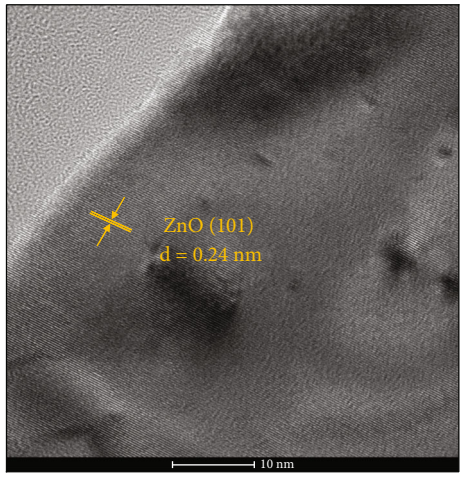

Figure 4: HRTEM image of the 3 at% Ag-functionalized porous ZnO sheets.

optimized in a sensor fabricated with 3 at% Ag-functionalized porous ZnO sheets at 200°C. Possible mechanisms for enhanced sensing properties in this hybrid materials were also discussed.

2. Experimental

2.1. Synthesis of Ag-Functionalized Porous ZnO Sheets. Initially, 0.02 mol $Zn(NO)_3{\cdot}6H_2O$ and 0.06 mol urea were completely dissolved in a 180 mL mixture of ethanol–water (1 : 2, v–v) via mixing for 30 min. Then, 0.06, 0.12, and 0.18 g $AgNO_3$ (1, 3, and 5 at% Ag) were added to the solution, and a transparent mixed solution (zinc nitrate hexahydrate + urea + silver nitrate in ethanol-water) was obtained. This solution was poured into a 250 mL Teflon-lined autoclave and maintained at 180°C for 24 h. After this, the white precipitate was collected and washed several times with deionized water and absolute ethanol by centrifugation. Next, the precipitate was dried under vacuum at 80°C for 6 h. Finally, the Ag-functionalized porous ZnO sheets were obtained after annealing under Ar flow at 550°C for 4 h. The corresponding schematic is shown in Figure 1.

2.2. Characterization. Crystallinity and phases were examined by X-ray diffraction (XRD, SmartLab, Rigaku) with CuKα radiation ($\lambda = 1.541$ Å). Morphology was analyzed using a transmission electron microscope (TEM, Talos F200X, FEI). An energy dispersive X-ray spectrometer (EDS, Talos F200X, FEI) incorporated into the TEM was used to verify chemical composition. X-ray photoelectron spectroscopy (XPS, Thermo Fisher Scientific Co.) was employed to investigate the chemical states using the C 1 s peak (284.8 eV) as a reference. Photoluminescence (PL, Ram Boss, Dongwoo Optron) was evaluated using a He–Cd laser with 325 nm excitation wavelength.

2.3. Gas Sensing Test. Au interdigitated electrodes were sputter-deposited on the surface of an alumina substrate. Sputtering was performed at 80 mA for 12 min, and the final thickness of the electrodes was 300 nm. The fabricated gas sensor was placed on a ceramic heater, and its gas sensing properties were measured using a lab-made gas sensing system (Supplementary Materials (SM), Figure S1). Desired amounts of target gases were mixed with dry synthetic air as a background using mass flow controllers (MFCs). The resistance of the gas sensor in air (R_a) and in the existence of the target gas (R_g) was checked using a multimeter. The response was calculated as $R = R_g/R_a$ for oxidizing gases and $R = R_a/R_g$ for reducing gases. The response time was calculated as the time needed for the sensor to reach 90% of the final resistance in the presence of NO_2 gas. Furthermore, the recovery time was evaluated as the time required for the sensor to reach 90% of the final resistance after stoppage of the NO_2 gas flow.

3. Results and Discussions

3.1. Morphological, Chemical, and Structural Studies. Figures 2(a)–2(f) indicate the TEM images of 1, 3, and 5 at% Ag-functionalized porous ZnO sheets, respectively. Interestingly, sheet-like ZnO with highly dense pore, which is desirable for sensing applications due to the large surface area, was formed. Dark particles represent the Ag particles functionalized on the surface of ZnO. Figures 3(a)–3(o)show the TEM elemental mapping data of 1, 3, and 5 at% Ag-functionalized porous ZnO sheets, respectively. Zn and O are evenly distributed over the sheet surface, whereas Ag is localized in certain places. Specifically in Figures 3(e), 3(j), and 3(o), it can be clearly observed that the dark points are pores, and the yellow points are Ag particles, which ensures the formation of Ag-functionalized porous ZnO sheets. The TEM–EDS point analysis results of 1, 3, and 5 at% Ag-functionalized porous ZnO sheets are given in SM Figure S2(a–d), (e–h), and (i-l), respectively. The white area in SM, Figure S2(a and b) is mostly rich in Ag, whereas the gray area in SM, Figure S2 (c and d) is rich in ZnO. Similarly, in SM, Figure S2 (e and f) and SM, Figure S2(i and j), a white area with 99.8 wt% Ag and 98.9 wt% Ag is recorded, whereas in SM, Figure S2(g and h) and SM, Figure S2(k and l), a gray area with 88.6 wt% Zn and 90.0 wt% Zn is observed. Overall, the TEM–EDS point analysis results confirmed the formation of Ag-functionalized porous ZnO sheets. SM, Figure S3(a) shows the XRD patterns of 3 at% Ag-functionalized porous ZnO sheets. Standard JCPDS files of Ag and ZnO are also shown in SM, Figure S3(b and c) for comparison. In both cases, the peaks related to both Ag and ZnO according to the JCPDS file nos. 04-0783 and 36-1451 were observed [27] without impurities. The crystallinity in XRD shows good agreement with HRTEM (Figure 4). Figure 5(a) indicates the XPS survey of 3 at% Ag-functionalized porous ZnO sheets, revealing the presence of all expected elements, namely, Zn, Ag, and O (peak related to C is due to the environment). The high-resolution Zn 2p core-level region is shown in Figure 5(b), where the two peaks at the binding energies of 1022.38 and 1045.38 eV are attributed to Zn $2p_{1/2}$ and Zn $2p_{3/2}$, respectively, with a spin-orbit splitting of 23.03 eV, which is in accordance with the previously reported

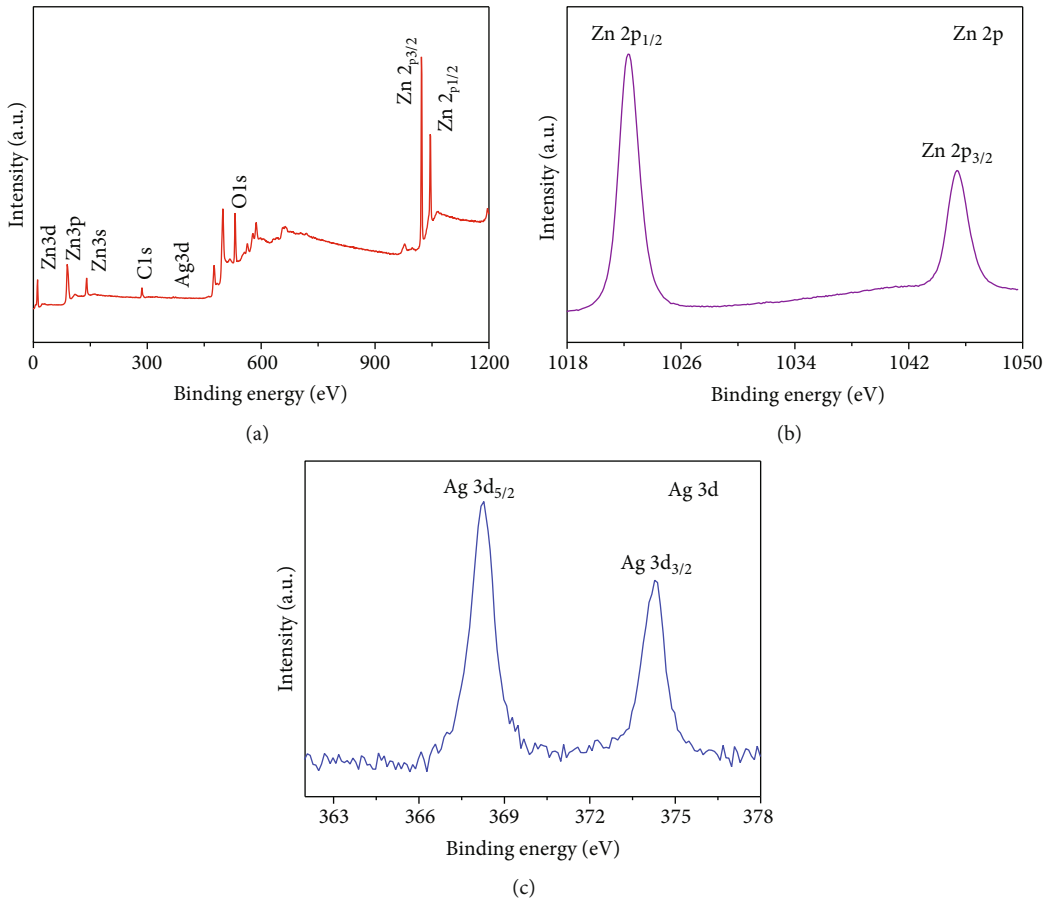

FIGURE 5: (a) XPS survey of the 3 at% Ag-functionalized porous ZnO sheets and high-resolution XPS core-levels of (b) Zn 2p and (c) Ag 3d.

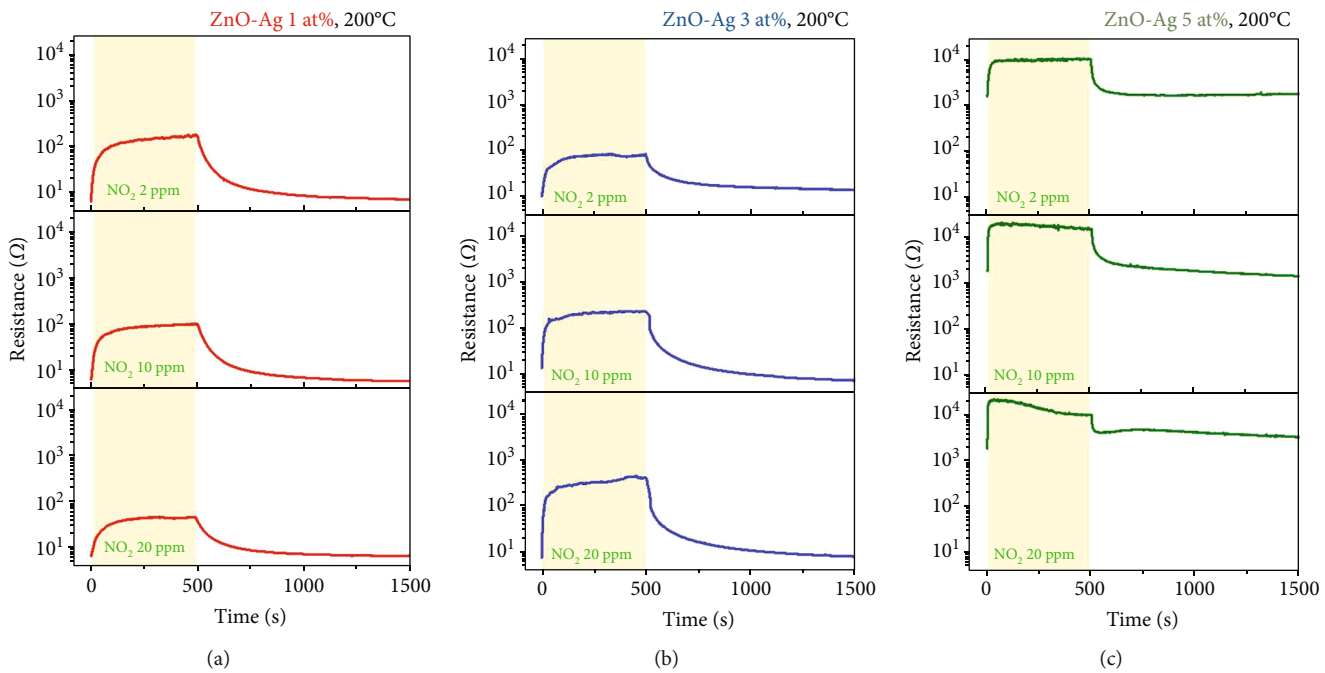

FIGURE 6: Dynamic resistance curves of the (a) 1, (b) 3, and (c) 5 at% Ag-functionalized porous ZnO sheet gas sensor at 200°C to 2, 10, and 20 ppm NO_2 gas.

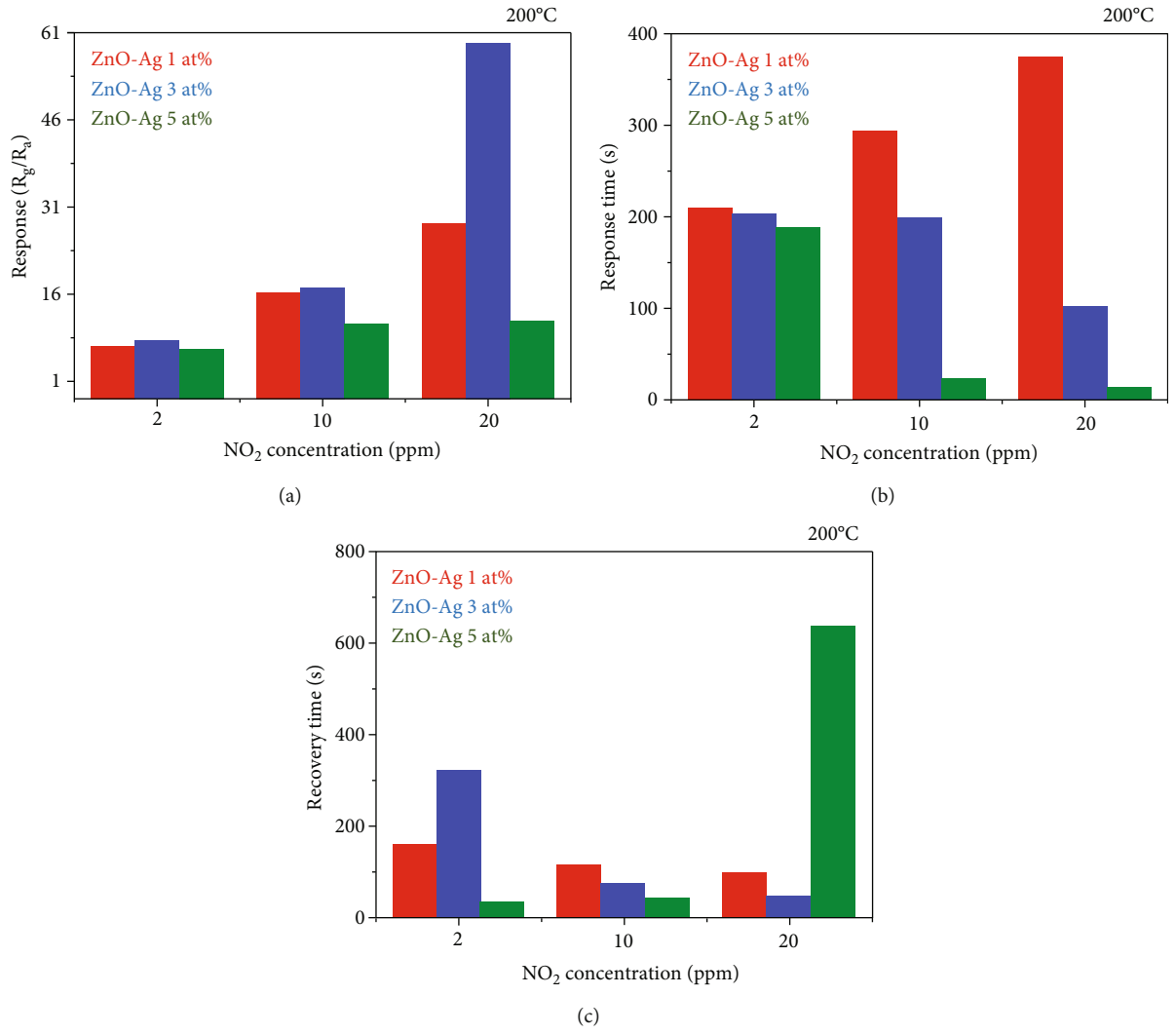

Figure 7: (a) Response, (b) response time, and (c) recovery time of the 1, 3, and 5 at% Ag-functionalized porous ZnO sheet gas sensors to NO_2 gas at 200°C.

Table 1: Response, response time, and recovery time of 1, 3, and 5 at% Ag-functionalized porous ZnO sheets gas sensors to different concentrations of NO_2 gas at 200°C.

	ZnO-Ag 1 at%			ZnO-Ag 3 at%			ZnO-Ag 5 at%		
	2 ppm	10 ppm	20 ppm	2 ppm	10 ppm	20 ppm	2 ppm	10 ppm	20 ppm
Response (R_g/R_a)	7.11	16.29	28.16	8.04	17.18	59.26	6.62	10.86	11.40
Response time (s)	210	294	375	203	199	102	189	23	14
Recovery time (s)	160	116	100	323	75	49	35	43	638

literature [33]. This indicates that Zn is in the Zn^{2+} oxidation state [34, 35]. Figure 5(c) shows the high-resolution Ag 3d core-level region, where the Ag 3d $_{3/2}$ and Ag 3d $_{5/2}$ peaks can be observed at the binding energies of 374.28 and 368.28 eV, in accordance with the literature [36].

SM, Figure S4 shows the PL spectrum of 3 at% Ag-functionalized porous ZnO sheets. Based on literature, the PL spectrum of ZnO indicates a band emission in the ultraviolet (UV) region and a broad defect emission in the visible range [37]. The UV emission is owing to the near-band-edge emission of ZnO, which results from the recombination of free excitons through an exciton–exciton collisions [38]. Emissions in the visible region are because of the recombination of different defects [37].

3.2. Gas Sensing Studies. We measured the resistance of the gas sensors at 100, 200, and 300°C and found the optimum operating temperature of 200°C. Figures 6(a)–6(c) show the dynamic resistance curves of (Figure 6(a)) 1, (Figure 6(b)) 3, and (Figure 6(c)) 5 at% Ag-functionalized

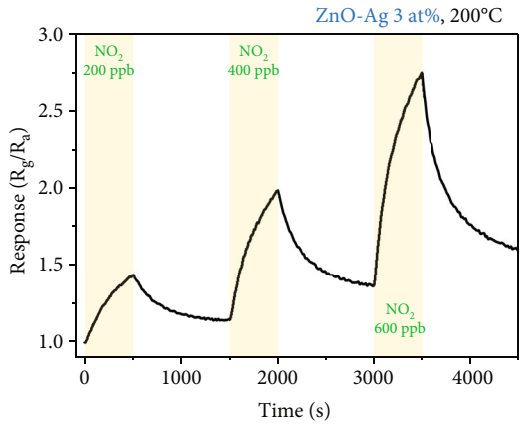

Figure 8: Response curves of the 3 at% Ag-functionalized porous ZnO sheets with 200, 400, and 600 ppb NO_2 gas concentration at 200°C.

porous ZnO sheet gas sensors at various concentrations of NO_2 gas at 200°C, respectively. The sensors exhibit *n*-type semiconducting behavior due to the *n*-type nature of ZnO. Different sensor parameters including response, response time, and recovery time were calculated and shown in Figure 7 and Table 1. The response of the 3 at% Ag-functionalized porous ZnO sheet sensor (8.04, 17.18, and 59.26 for 2, 10, and 20 ppm NO_2 gases, respectively) was higher than those of the 1 at% (7.11, 16.29, and 28.16 for 2, 10, and 20 ppm NO_2 gases, respectively) and 5 at% (6.62, 10.86, and 11.40 for 2, 10, and 20 ppm NO_2 gases, respectively) Ag-functionalized porous ZnO sheets sensors at all NO_2 gas concentrations (Figure 7(a)). Interestingly, the response time of the 3 at% Ag-functionalized porous ZnO sheet sensor (203, 199, and 102 s for 2, 10, and 20 ppm NO_2 gases, respectively) was shorter than that of the 1 at% Ag-functionalized porous ZnO sheet sensor (210, 294, and 375 s for 2, 10, and 20 ppm NO_2 gases, respectively) but longer than that of the 5 at% Ag-functionalized porous ZnO sheets sensor (189, 23, and 14 s for 2, 10, and 20 ppm NO_2 gases, respectively), at all NO_2 gas concentrations (Figure 7(b)). A comparison of the recovery times of three gas sensors is shown in Figure 7(c). As the 3 at% Ag-functionalized porous ZnO sheet sensor demonstrated a higher response to NO_2 gas, it was selected for further studies. In fact, ppb-based low concentration of NO_2 gas can be detected but their responses were too low as seen in Figure 8. Figures 9(a) and 9(b) show the dynamic response graphs of ZnO-Ag 3at% sensor and presents the relevant selectivity to 10 ppm of various gases at 200°C. The response of the gas sensor to 10 ppm of NO_2, H_2S, C_6H_6, SO_2, and C_7H_8 gases was 17.18, 3.75, 2.74, 2.32, and 2.22, respectively. This demonstrates the good selectivity of optimal gas sensor. In addition, Figures 9(c) and 9(d) show the resistance of the patterned ZnO-Ag 3at % sensor to 10 ppm of NO_2, 0, 30, and 60% relative humidity at 200°C. The basic condition is that all gases are dry. However, in an actual environment, the target gas is inevitably a gas containing moisture that is always present in the atmosphere. Therefore, dry air was allowed to pass through the bubble system to control the humidity of the dry gas. That is, by controlling the humidity in the RH probe hygrometer, wet air can meet dry target gas, so the change in response of gas sensing can be observed at all gas humidity. However, it should be noted that the initial resistance may change, as seen in Figure 9(c), depending on the humidity. In other words, even if the gas sensing process temperature (200°C) is the same, since the relative humidity of the initial gases entering the chamber is different, it is possible to have different initial resistances. Due to the following reactions, electron and oxygen vacancy (V_o) increase in *n* -type ZnO, so the initial base line further decreases compared to the dry gas state (Figure 9(c)) [39, 40].

$$H_2O + Zn + O \longrightarrow (HO - Zn) + OH + e^-, \quad (1)$$

$$H + O^{2-} \longrightarrow (OH)^- + e^-, \quad (2)$$

$$H_2O + 2Zn + O \longrightarrow 2(HO - Zn) + V_o. \quad (3)$$

Therefore, in order to investigate the effect of humidity, it is reasonable to compare the difference in response as shown in Figure 9(d). The responses to 10 ppm NO_2 gas at 0, 30, and 60% relative humidity at 200°C were 17.18, 15.21, and 14.05, respectively. Even in the humid environment, the sensor can reliably detect low concentrations of NO_2 gas. Finally, regarding the performance of gas sensing, even if measured after 3 months, the response value decreases, but there seems to be no problem with the long-term use of gas sensing (Figures 9(e) and 9(f)). Then, the responses to 10 ppm NO_2 gas at 200°C in a fresh state and after three months were 17.18 and 4.37, respectively.

3.3. Sensing Mechanisms. The basic sensing mechanism conductometric gas sensors are the modulation of the resistance of the sensing layer in the existence of the target gas [41, 42]. Initially, in air, when gas sensors are exposed to an oxygen environment, oxygen adsorbs electrons from the surface of ZnO because of its high electron affinity and is converted to ionic species as follows [43, 44]:

$$O_2(g) \longrightarrow O_2(\text{ads}), \quad (4)$$

$$O_2(\text{ads}) + e^- \longrightarrow O_2^-(\text{ads}), \quad (5)$$

$$O_2^-(\text{ads}) + e^- \longrightarrow O^-, \quad (6)$$

$$O^- + e^- \longrightarrow O^{2-}. \quad (7)$$

Due to the abstraction of electrons by the adsorbed oxygen species, an electron depletion layer (EDL) is developed on the ZnO surface, where a higher resistance relative to that of the core parts is expected owing to the lower concentrations of electrons. When NO_2 gas is injected into the gas chamber, the surface EDL expands because NO_2 has a higher electron affinity (2.28 eV) than oxygen (0.43 eV) and leads to an increase in the resistance of the gas sensor [45]. The relevant reactions are as follows [46]:

$$NO_2 + e^- \longrightarrow NO_2^-, \quad (8)$$

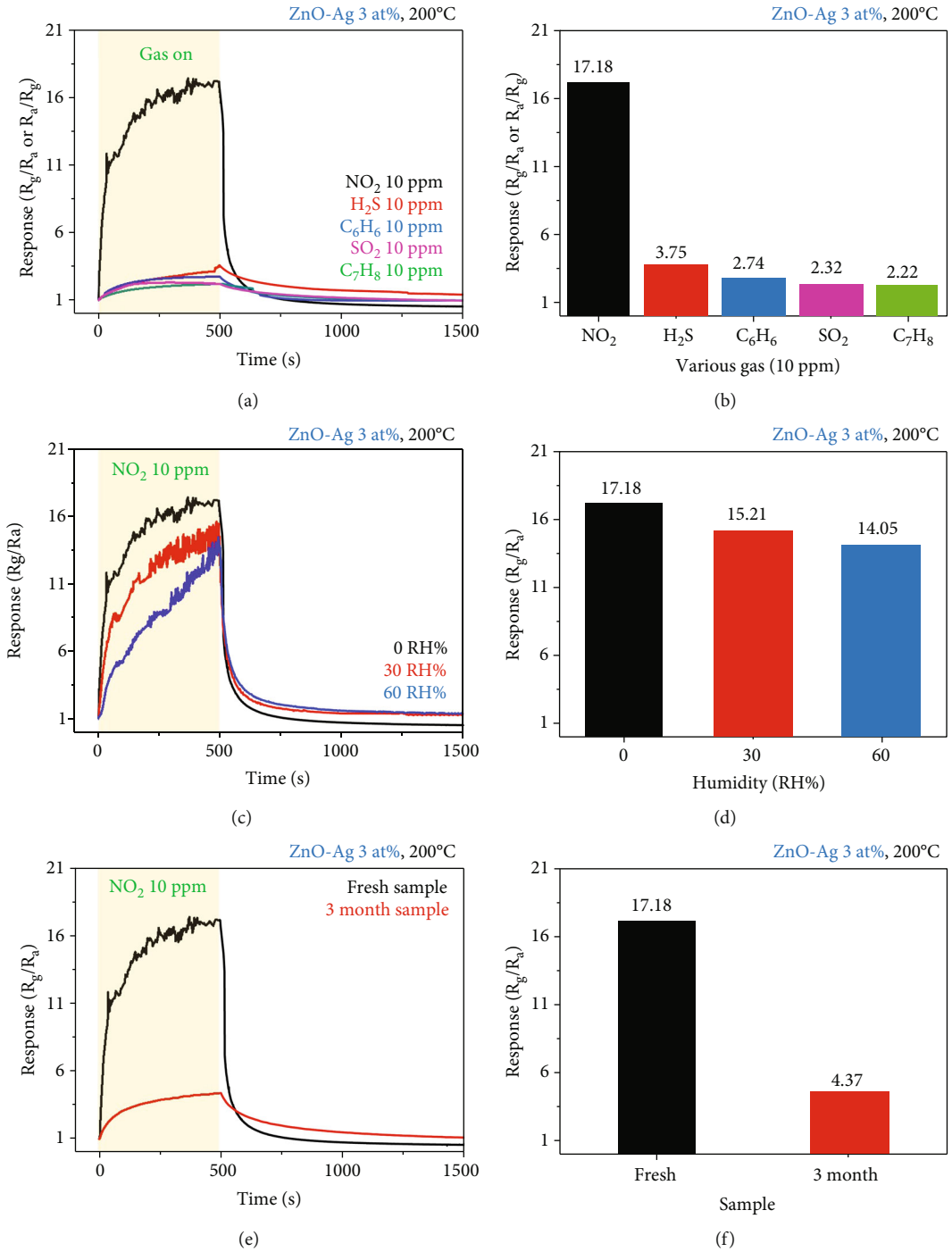

Figure 9: (a) Dynamic response curves of the 3 at% Ag-functionalized porous ZnO sheet gas sensor to 10 ppm of various gases at 200°C. (b) Selectivity pattern of (a, c). Dynamic resistance curve of the 3 at% Ag-functionalized porous ZnO sheet gas sensor in the presence of 30% RH and 60% RH. (d) Response comparison of 10 ppm NO_2 gas sensor in dry and humid atmospheres. (e) Dynamic response curve of the 3 at% Ag-functionalized porous ZnO sheet gas sensor after three months. (f) Comparison between the response of the gas sensor to 10 ppm NO_2 in a fresh state and after three months.

$$NO_2 + e^- \longrightarrow NO + O^-, \quad (9)$$

$$NO_2^- + O^- + 2e^- \longrightarrow NO + 2O^{2-}. \quad (10)$$

Furthermore, in the homojunctions between ZnO sheets, potential barriers are initially formed in air, and upon exposure to NO_2 gas, the height of these potential barriers increases due to the further abstraction of electrons, contributing to the sensing signal.

In addition, the effects of Ag on the gas sensing characteristics of ZnO sheets were investigated. Owing to the differences between the work functions of Ag (4.72 eV) and

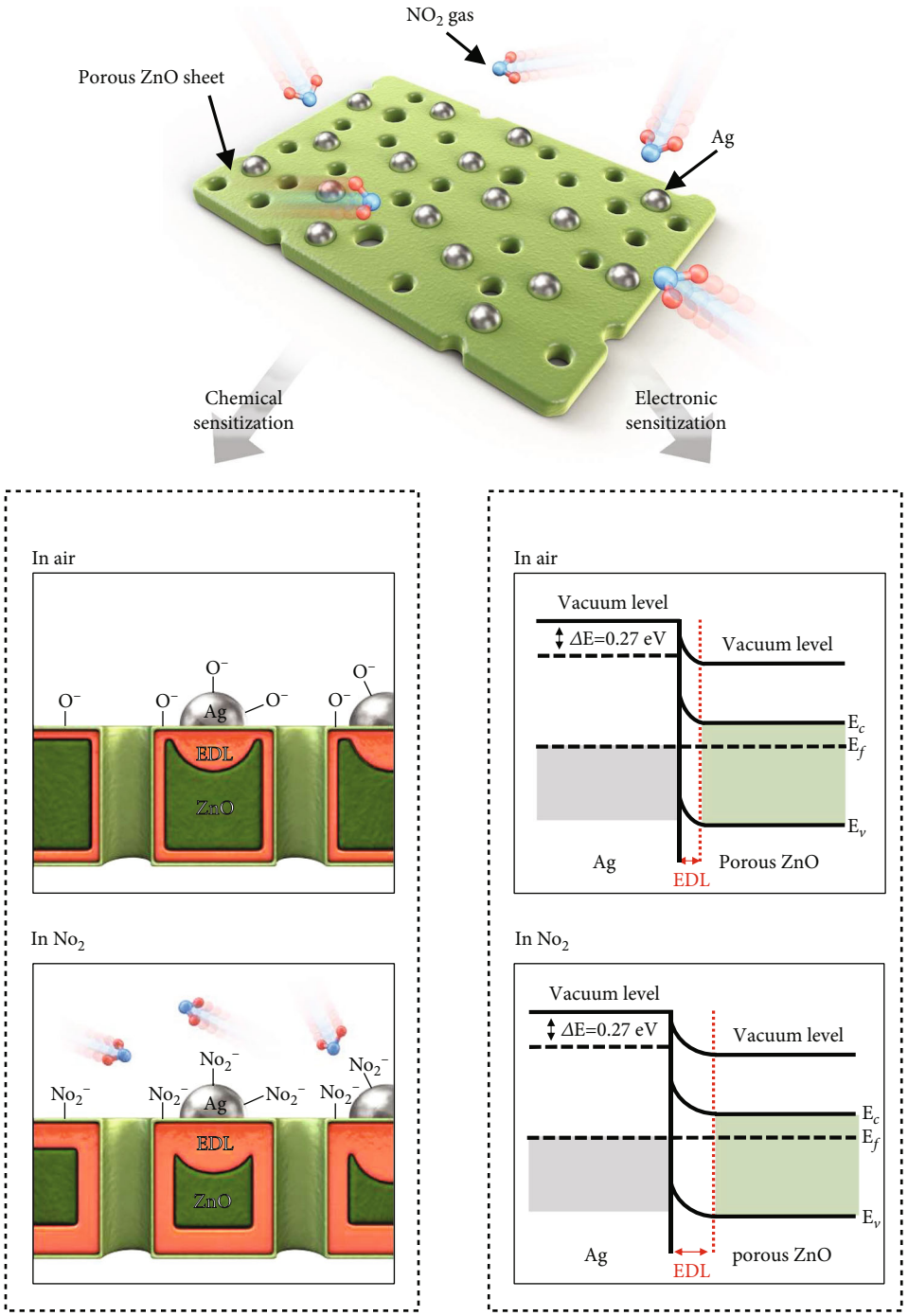

Figure 10: Schematic of the NO_2 sensing mechanism of Ag-functionalized porous ZnO sheets.

ZnO (4.45 eV) [47], the electrons transfer from ZnO to Ag, resulting in intimate contacts between Ag and ZnO to equate the Fermi levels. Accordingly, a Schottky barrier is formed near the interfaces of ZnO and Ag in air. This increases the resistance of the gas sensor as compared to that of pristine ZnO sheets. Upon exposure to NO_2 gas and further extraction of electrons from the surface of ZnO, the width and height of the Schottky barriers increase, leading to higher resistance of the gas sensor in the presence of Ag particles. This effect is an electronic effect or electronic sensitization of Ag. In other words, as the content of Ag increases, the initial resistance of the ZnO sheets may increase because more Schottky barriers are formed as seen in Figure 6. In another effect, similar to Au [48], Ag catalytically decomposes the oxygen molecules into atomic species when they come in contact with the surface of Ag particles. Then, owing to the so-called spill-over effect, the oxygen atoms move to the surface of neighboring ZnO and easily adsorb on this surface [49]. Therefore, more oxygen species adsorb on the surface of ZnO, and their more reactions with NO_2 lead to a higher response of the sensor to NO_2 gas. In addition, because of the process temperature of 200°C,

Table 2: Comparison between the NO_2 gas sensing properties of ZnO-based gas sensors with the present optimized gas sensor.

Sensor	NO_2 conc. (ppm)	Response (R_g/R_a)	Temp. (°C)	Ref.
Au-decorated ZnO-branched SnO_2 NWs	10	13.07	300	[24]
Co-decorated ZnO branched SnO_2 NWs	10	7.48	300	[51]
ZnO@Au miscrospheres	1	17	250	[46]
1 mol% Pd-ZnO NWs	1	13.5	100	[52]
Ni-doped ZnO thin film	5	2.08	200	[53]
ZnO nanosheet arrays	100	19	180	[54]
ZnO nanoparticles	100	6.86	150	[55]
ZnO nanorods	0.001	1.3	150	[56]
Al-doped ZnO nanorods	5	0.86	175	[57]
	2	8.04		
3 at% Ag-functionalized porous ZnO sheets	10	17.18	200	Present work
	20	59.26		

oxygen species can react with Ag to form Ag_2O, but even at this time, electrons are transferred from ZnO to Ag_2O to play a role in increasing the resistance of ZnO [50]. Figure 10 schematically shows the sensing mechanism of the 3 at% Ag-functionalized sensor. Table 2 presents a comparison between the NO_2 sensing capacities of ZnO-based gas sensors reported in the literature and the present optimized sensor [24, 46, 51–57]. It can be observed that the present sensor has good performance when compared with the performances of other relevant gas sensors mainly because of the catalytic effect of Ag, formation of Ag/ZnO Schottky contacts, and high surface area due to the porous nature of the synthesized sheet, where the gas molecules can diffuse into the deep parts of the sheets.

4. Conclusions

We proposed the hydrothermal route to prepare hybrid materials of Ag and ZnO. Submicron Ag particles functionalized porous ZnO sheets were formed during the chemical reaction between Zn and Ag precursors in a mixed solution of ethanol and water. From the designed measurements of NO_2 gas sensing properties of the sensors fabricated with Ag-functionalized porous ZnO sheets, we found that response and recovery time can be simultaneously improved by the hybridization of Ag particles due to the chemical and electrical sensitization effects even under high-humidity atmosphere. The 3 at% Ag-functionalized porous ZnO sheet sensor represents response of 17.18 and response time of 199 s under 10 ppm NO_2 gas at 200°C and shows good selectivity. We believe that researches based on our synthetic approach will provide enhanced sensing properties in any oxide-based gas sensing materials and expand the applications of semiconductor metal oxide gas sensors.

Data Availability

All the data are available from the corresponding authors on reasonable request.

Disclosure

An earlier version of preprint on the manuscript has been presented as Research Square according to the following link https://papers.ssrn.com/sol3/papers.cfm?abstract_id=4227509.

Conflicts of Interest

The authors declare no competing interests.

Authors' Contributions

Min Young Kim and Jeong Yun Hwang had equal contribution as co-first authors.

Acknowledgments

This study was supported by Samsung Electronics Co., Ltd. (IO201216-08204-01). This research was also supported by the Basic Science Research Program through the National Research Foundation of Korea (NRF) funded by the Ministry of Science and ICT (2022R1A2C2005210) and the Ministry of Education (2019R1A6A1A11055660). Seung Yong Lee and Changhyun Jin were supported by the Korea Initiative for fostering University of Research and Innovation (KIURI) Program of the National Research Foundation (NRF) funded by the Korea government (MSIT) (NRF-2020M3H1A1077207).

Supplementary Materials

Supplementary data associated with this article can be found in the Supplementary Information. (Supplementary Materials). Figure S1: (a) schematic diagram of gas sensor system. (b) Actual image of the sensor chamber. Figure S2: TEM–EDS point analysis of the (a–d) 1, (e–h) 3, and (i-l) 5 at% Ag-functionalized porous ZnO sheets. Figure S3: XRD analysis. JCPDS card patterns of (a) ZnO and (b) Ag. XRD patterns of (c) the 3 at% Ag-functionalized porous ZnO sheets. Figure S4: PL spectrum of the 3 at% Ag-functionalized porous ZnO sheets. *(Supplementary Materials)*

References

[1] R. Kumar, O. Al-Dossary, G. Kumar, and A. Umar, "Zinc oxide nanostructures for NO_2 gas–sensor applications: a review," *Nano-Micro Letters*, vol. 7, no. 2, pp. 97–120, 2015.

[2] S. Kumar, V. Pavelyev, P. Mishra, N. Tripathi, P. Sharma, and F. Calle, "A review on 2D transition metal di-chalcogenides and metal oxide nanostructures based NO_2 gas sensors," *Materials Science in Semiconductor Processing*, vol. 107, article 104865, 2020.

[3] S. W. Lee, W. Lee, Y. Hong, G. Lee, and D. S. Yoon, "Recent advances in carbon material-based NO_2 gas sensors," *Sensors and Actuators B: Chemical*, vol. 255, pp. 1788–1804, 2018.

[4] Y. Wu, N. Joshi, S. Zhao et al., "NO_2 gas sensors based on CVD tungsten diselenide monolayer," *Applied Surface Science*, vol. 529, article 147110, 2020.

[5] M. T. Jijjapu, S. G. Surya, S. Yuvaraja, X. Zhang, H. N. Alshareef, and K. N. Salama, "Fully integrated indium gallium zinc oxide NO2Gas detector," *ACS Sensors*, vol. 5, no. 4, pp. 984–993, 2020.

[6] X. Geng, P. Lu, C. Zhang, D. Lahem, M.-G. Olivier, and M. Debliquy, "Room-temperature NO_2 gas sensors based on $_{1-x}$ composites: Experiments and molecular dynamics simulation," *Sensors and Actuators B: Chemical*, vol. 282, pp. 690–702, 2019.

[7] A. Mirzaei, K. Janghorban, B. Hashemi, M. Bonyani, S. G. Leonardi, and G. Neri, "A novel gas sensor based on Ag/Fe_2O_3 core-shell nanocomposites," *Ceramics International*, vol. 42, no. 16, pp. 18974–18982, 2016.

[8] S. K. Shaikh, V. V. Ganbavale, S. V. Mohite, U. M. Patil, and K. Y. Rajpure, "ZnO nanorod based highly selective visible blind ultra-violet photodetector and highly sensitive NO_2 gas sensor," *Superlattices and Microstructures*, vol. 120, pp. 170–186, 2018.

[9] V. L. Patil, S. A. Vanalakar, N. L. Tarwal et al., "Construction of cu doped ZnO nanorods by chemical method for low temperature detection of NO_2 gas," *Sensors and Actuators A: Physical*, vol. 299, article 111611, 2019.

[10] T. Seiyama, A. Kato, K. Fujiishi, and M. Nagatani, "A new detector for gaseous components using semiconductive thin films," *Analytical Chemistry*, vol. 34, no. 11, pp. 1502-1503, 1962.

[11] J. Wang, M. Yu, Y. Xia, X. Li, C. Yang, and S. Komarneni, "On-chip grown ZnO nanosheet-array with interconnected nanojunction interfaces for enhanced optoelectronic NO_2 gas sensing at room temperature," *Journal of Colloid and Interface Science*, vol. 554, pp. 19–28, 2019.

[12] J. Wang, Y. Shen, X. Li, Y. Xia, and C. Yang, "Synergistic effects of UV activation and surface oxygen vacancies on the room-temperature NO_2 gas sensing performance of ZnO nanowires," *Sensors and Actuators B: Chemical*, vol. 298, article 126858, 2019.

[13] Y. Zhou, C. Gao, and Y. Guo, "UV assisted ultrasensitive trace NO2gas sensing based on few-layer MoS2nanosheet–ZnO nanowire heterojunctions at room temperature," *Journal of Materials Chemistry A*, vol. 6, no. 22, pp. 10286–10296, 2018.

[14] R. Chen, J. Wang, Y. Xia, and L. Xiang, "Near infrared light enhanced room-temperature NO_2 gas sensing by hierarchical ZnO nanorods functionalized with PbS quantum dots," *Sensors and Actuators B: Chemical*, vol. 255, pp. 2538–2545, 2018.

[15] H.-J. Choi, S.-H. Kwon, W.-S. Lee et al., "Ultraviolet photoactivated room temperature NO_2 gas sensor of ZnO hemitubes and nanotubes covered with TiO_2 nanoparticles," *Nanomaterials*, vol. 10, no. 3, p. 462, 2020.

[16] A. Sanger, S. B. Kang, M. H. Jeong, C. U. Kim, J. M. Baik, and K. J. Choi, "All-transparent NO2gas sensors based on free-standing Al-doped ZnO nanofibers," *ACS Applied Electronic Materials*, vol. 1, no. 7, pp. 1261–1268, 2019.

[17] R. K. Sonker, S. Sabhajeet, S. Singh, and B. J. M. L. Yadav, "Synthesis of ZnO nanopetals and its application as NO_2 gas sensor," *Materials Letters*, vol. 152, pp. 189–191, 2015.

[18] S. Arunkumar, T. Hou, Y.-B. Kim et al., "Au decorated ZnO hierarchical architectures: facile synthesis, tunable morphology and enhanced CO detection at room temperature," *Sensors and Actuators B: Chemical*, vol. 243, pp. 990–1001, 2017.

[19] Y. Mun, S. Park, S. An, C. Lee, and H. W. Kim, "NO_2 gas sensing properties of Au-functionalized porous ZnO nanosheets enhanced by UV irradiation," *Ceramics International*, vol. 39, no. 8, pp. 8615–8622, 2013.

[20] L. Qi, L. Yu, Z. Liu, F. Guo, Y. Q. Gu, and X. Fan, "An enhanced optoelectronic NO_2 gas sensors based on direct growth ZnO nanowalls in situ on porous rGO," *Journal of Alloys and Compounds*, vol. 749, pp. 244–249, 2018.

[21] V. Ramakrishnan, K. G. Nair, J. Dhakshinamoorthy, K. R. Ravi, and B. Pullithadathil, "Porous, n–p type ultra-long, $_{ZnO@-Bi2O3heterojunction}$ nanorods - $_{based}$ NO2gas sensor: new insights towards charge transport characteristics," *Physical Chemistry Chemical Physics*, vol. 22, no. 14, pp. 7524–7536, 2020.

[22] Y. Wei, X. Wang, G. Yi et al., "Hydrothermal synthesis of Ag modified ZnO nanorods and their enhanced ethanol- sensing properties," *Materials Science in Semiconductor Processing*, vol. 75, pp. 327–333, 2018.

[23] T. Dilova, G. Atanasova, A. Og et al., "Effect of Pd-decoration on the sensing properties of ZnO nanostructures," *Thin Solid Films*, vol. 693, article 137693, 2020.

[24] M. S. Choi, J. H. Bang, A. Mirzaei et al., "Promotional effects of ZnO-branching and au-functionalization on the surface of SnO_2 nanowires for NO_2 sensing," *Alloys and Compounds*, vol. 786, pp. 27–39, 2019.

[25] D. Liu, J. Pan, J. Tang, W. Liu, S. Bai, and R. Luo, "Ag decorated SnO_2 nanoparticles to enhance formaldehyde sensing properties," *Journal of Physics and Chemistry of Solids*, vol. 124, pp. 36–43, 2019.

[26] A. Mirzaei, K. Janghorban, B. Hashemi, and G. Neri, "Metal-core@metal oxide-shell nanomaterials for gas-sensing applications: a review," *Journal of Nanoparticle Research*, vol. 17, no. 9, p. 371, 2015.

[27] Z. Yin, X. Wang, F. Sun et al., "Aligned hierarchical Ag/ZnO nano-heterostructure arrays via electrohydrodynamic nanowire template for enhanced gas-sensing properties," *Scientific Reports*, vol. 7, no. 1, p. 12206, 2017.

[28] Y. Hu, T. Li, J. Zhang, J. Guo, W. Wang, and D. Zhang, "High-sensitive NO_2 sensor based on p-$NiCo_2O_4$/n-WO_3 heterojunctions," *Sensors and Actuators B: Chemical*, vol. 352, article 130912, 2022.

[29] D. Wang, D. Zhang, J. Guo et al., "Multifunctional poly(vinyl alcohol)/ag nanofibers-based triboelectric nanogenerator for self-powered MXene/tungsten oxide nanohybrid NO_2 gas sensor," *Nano Energy*, vol. 89, article 106410, 2021.

[30] Y. Yang, D. Zhang, D. Wang, Z. Xu, and J. Zhang, "A high-stability weighing paper/polytetrafluoroethylene-based

triboelectric nanogenerator for self-powered $_{In2O3nanocubes/SnS2nanoflower}$ NO2gas sensors," *Journal of Materials Chemistry A*, vol. 9, no. 25, pp. 14495–14506, 2021.

[31] Z. Yang, D. Zhang, and H. Chen, "MOF-derived indium oxide hollow microtubes/MoS_2 nanoparticles for NO_2 gas sensing," *Sensors and Actuators B: Chemical*, vol. 300, article 127037, 2019.

[32] T. Li, D. Zhang, Q. Pan, M. Tang, and S. Yu, "UV enhanced NO_2 gas sensing at room temperature based on coral-like tin diselenide/MOFs-derived nanoflower-like tin dioxide heteronanostructures," *Sensors and Actuators B: Chemical*, vol. 355, article 131049, 2022.

[33] G. L. Kabongo, G. H. Mhlongo, B. M. Mothudi, K. T. Hillie, P. S. Mbule, and M. S. Dhlamini, "Structural, photoluminescence and XPS properties of Tm^{3+} ions in ZnO nanostructures," *Journal of Luminescence*, vol. 187, pp. 141–153, 2017.

[34] V. Kumar, H. C. Swart, O. M. Ntwaeaborwa et al., "Origin of the red emission in zinc oxide nanophosphors," *Materials Letters*, vol. 101, pp. 57–60, 2013.

[35] F. C. Correia, N. Bundaleski, O. M. N. D. Teodoro et al., "XPS analysis of ZnO:Ga films deposited by magnetron sputtering: substrate bias effect," *Applied Surface Science*, vol. 458, pp. 1043–1049, 2018.

[36] Y. L. Mikhlin, G. A. Pal'yanova, Y. V. Tomashevich, E. A. Vishnyakova, S. A. Vorobyev, and K. A. Kokh, "XPS and Ag L_3-edge XANES characterization of silver and silver-gold sulfoselenides," *Journal of Physics and Chemistry of Solids*, vol. 116, pp. 292–298, 2018.

[37] H. W. Kim, Y. J. Kwon, A. Mirzaei et al., "Synthesis of zinc oxide semiconductors-graphene nanocomposites by microwave irradiation for application to gas sensors," *Sensors and Actuators B: Chemical*, vol. 249, pp. 590–601, 2017.

[38] C. C. Wang, F. S. Shieu, and H. C. Shih, "Ag-nanoparticle enhanced photodegradation of ZnO nanostructures: investigation using photoluminescence and ESR studies," *Journal of Environmental Chemical Engineering*, vol. 9, article 104707, 2020.

[39] C.-L. Hsu, L.-F. Chang, and T.-J. Hsueh, "Light-activated humidity and gas sensing by ZnO nanowires grown on LED at room temperature," *Sensors and Actuators B: Chemical*, vol. 249, pp. 265–277, 2017.

[40] S. Vallejos, I. Gràcia, N. Pizúrová et al., "Gas sensitive ZnO structures with reduced humidity-interference," *Sensors and Actuators B: Chemical*, vol. 301, article 127054, 2019.

[41] A. Mirzaei, J.-H. Kim, H. W. Kim, and S. S. Kim, "Resistive-based gas sensors for detection of benzene, toluene and xylene (BTX) gases: a review," *Journal of Materials Chemistry C*, vol. 6, no. 16, pp. 4342–4370, 2018.

[42] A. Mirzaei, S. S. Kim, and H. W. Kim, "Resistance-based H_2S gas sensors using metal oxide nanostructures: a review of recent advances," *Journal of Hazardous Materials*, vol. 357, pp. 314–331, 2018.

[43] V. P. Dinesh, A. Sukhananazerin, and P. Biji, "An emphatic study on role of spill-over sensitization and surface defects on NO_2 gas sensor properties of ultralong heterojunction NRs," *Journal of Alloys and Compounds*, vol. 712, pp. 811–821, 2017.

[44] Y. H. Navale, S. T. Navale, F. J. Stadler, N. S. Ramgir, and V. B. Patil, "Enhanced NO_2 sensing aptness of ZnO nanowire/CuO nanoparticle heterostructure-based gas sensors," *Ceramics International*, vol. 45, no. 2, pp. 1513–1522, 2019.

[45] P. Rai, Y.-S. Kim, H.-M. Song, M.-K. Song, and Y.-T. Yu, "The role of gold catalyst on the sensing behavior of ZnO nanorods for CO and NO_2 gases," *Sensors and Actuators B: Chemical*, vol. 165, no. 1, pp. 133–142, 2012.

[46] Z. Zhang, M. Xu, L. Liu et al., "Novel SnO_2@ZnO hierarchical nanostructures for highly sensitive and selective NO_2 gas sensing," *Sensors and Actuators B: Chemical*, vol. 257, pp. 714–727, 2018.

[47] H. R. Yousefi, B. Hashemi, A. Mirzaei, H. Roshan, and M. H. Sheikhi, "Effect of ag on the ZnO nanoparticles properties as an ethanol vapor sensor," *Materials Science in Semiconductor Processing*, vol. 117, article 105172, 2020.

[48] D. Veeran Ponnuvelu, S. Abdulla, and B. Pullithadathil, "Highly monodispersed mesoporous, heterojunction micro- spheres for trace-level detection of NO_2 gas," *Microporous and Mesoporous Materials*, vol. 255, pp. 156–165, 2018.

[49] G. Namgung, Q. T. H. Ta, W. Yang, and J.-S. Noh, "Diffusion-driven Al-doping of ZnO nanorods and stretchable gas sensors made of doped ZnO nanorods/ag nanowires bilayers," *ACS Applied Materials & Interfaces*, vol. 11, no. 1, pp. 1411–1419, 2019.

[50] H. Wang, Q. Li, X. Zheng et al., "3D porous flower-like ZnO microstructures loaded by large-size ag and their ultrahigh sensitivity to ethanol," *Journal of Alloys and Compounds*, vol. 829, article 154453, 2020.

[51] H. W. Kim, H. G. Na, Y. J. Kwon, H. Y. Cho, and C. Lee, "Decoration of co nanoparticles on ZnO-branched SnO_2 nanowires to enhance gas sensing," *Sensors and Actuators B: Chemical*, vol. 219, pp. 22–29, 2015.

[52] X. Chen, Y. Shen, P. Zhou et al., "NO_2 sensing properties of one-pot-synthesized ZnO nanowires with Pd functionalization," *Sensors and Actuators B: Chemical*, vol. 280, pp. 151–161, 2019.

[53] V. Ganbavle, S. Inamdar, G. Agawane, J. Kim, and K. Rajpure, "Synthesis of fast response, highly sensitive and selective Ni:ZnO based NO_2 sensor," *Chemical Engineering Journal*, vol. 286, pp. 36–47, 2016.

[54] C. Xiao, T. Yang, M. Chuai, B. Xiao, and M. Zhang, "Synthesis of ZnO nanosheet arrays with exposed (100) facets for gas sensing applications," *Physical Chemistry Chemical Physics*, vol. 18, no. 1, pp. 325–330, 2016.

[55] V. L. Patil, S. A. Vanalakar, P. S. Patil, and J. H. Kim, "Fabrication of nanostructured ZnO thin films based NO_2 gas sensor via SILAR technique," *Sensors and Actuators B: Chemical*, vol. 239, pp. 1185–1193, 2017.

[56] A. Resmini, U. Anselmi-Tamburini, S. M. Emamjomeh, V. Paolucci, I. G. Tredici, and C. Cantalini, "The influence of the absolute surface area on the NO_2 and H_2 gas responses of ZnO nanorods prepared by hydrothermal growth," *Thin Solid Films*, vol. 618, pp. 246–252, 2016.

[57] V. L. Patil, D. S. Dalavi, S. B. Dhavale et al., "NO_2 gas sensing properties of chemically grown Al doped ZnO nanorods," *Sensors and Actuators B: Chemical*, vol. 340, article 113546, 2022.